Catalysis Today xxx (xxxx) xxx

Contents lists available at ScienceDirect

Catalysis Today

journal homepage: www.elsevier.com/locate/cattod

Catalytic decomposition of formic acid in a fixed bed reactor – an experimental and modelling study

Tom Winkler [a,b], Fabien Baccot [a], Kari Eränen [a], Johan Wärnå [a], Gerd Hilpmann [b], Rüdiger Lange [b], Markus Peurla [c], Irina Simakova [a,d], Henrik Grénman [a], Dmitry Yu. Murzin [a], Tapio Salmi [a,*]

[a] Åbo Akademi University, Johan Gadolin Process Chemistry Centre (PCC), Laboratory of Industrial Chemistry and Reaction Engineering (TKR), Turku/Åbo, Finland
[b] Technische Universität Dresden, Institut für Verfahrens, und Umwelttechnik, Professur für Chemische Verfahrens, und Anlagentechnik, Dresden, Germany
[c] University of Turku, Department of Industrial Physics and Astronomy, Laboratory of Electron Microscopy, Turku/Åbo Finland
[d] University of Novosibirsk, Boreskov Institute of Catalysis, Novosibirsk Russian Federation

ARTICLE INFO

Keywords:
Formic acid
Decomposition
Kinetics
Mass transfer
Dimerization
Modelling

ABSTRACT

Formic acid is one of the key components in green chemistry being involved in energy storage, production of chemical intermediates and fuel components. Therefore the knowledge of its stability is of crucial importance and a systematic study of its decomposition is needed. The kinetics of formic acid decomposition to hydrogen and carbon dioxide was investigated in a laboratory-scale fixed bed reactor at 150–225 °C and atmospheric pressure. Palladium nanoparticles deposited on porous active carbon Sibunit were used as the heterogeneous catalyst. The catalyst was characterized by nitrogen physisorption and high-resolution transmission electron microscopy. The average palladium nanoparticle size was 5–6 nm. The impacts of mass transfer resistance and formic acid dimerization were negligible under the reaction conditions. Prolonged experiments revealed that the catalyst had a good stability. Hydrogen and carbon dioxide were the absolutely dominant reaction products, whereas the amounts of carbon monoxide and water were negligible. The experimental data were described with three kinetic models: first order kinetics, two-step adsorption-reaction model and multistep adsorption-decomposition model of formic acid. The multistep model gave the best description of the data.

1. Introduction

1.1. Formic acid – production and use

Formic acid (methanoic acid, HCOOH, FA) is a standard chemical product, which is globally used in many different industries. Two routes are commonly applied for FA production. Hydrolysis of methyl formate is applied in the Kemira-Leonard process, but FA can also be obtained from formate salts by acidolysis [1]. Formate salts are formed as stoichiometric co-products in the aldol production through Cannizzaro reaction. Besides these classical production technologies, new technologies based on sustainable resources are under development, such as the production of FA by hydrogenation of carbon dioxide [2]. This reaction presents the reverse route of the decomposition of FA. Consequently, it is conceivable to incorporate FA into a cyclic process. The OxFA process is another option for sustainable FA production: biomass is partially oxidised under mild conditions. The catalyst used for this process is a Keggin-type polyoxometallate [3].

Several industrial processes deploy formic acid (FA) as a substantial chemical component. FA is used in agriculture as an additive for animal feed, in leather production for tanning processes and in rubber production as a coagulant. Also new innovative processes use FA. For example, FA is supposed to be an important energy carrier for hydrogen storage [4]. Hydrogen is an efficient energy carrier [5], because it has a high energy density per mass, but a very low energy density per volume. Thus, energy production from hydrogen is very effective, but storage and transportation are quite challenging [6]. Therefore, the transformation to an alternative hydrogen storage medium is considered as an option to solve this problem. FA is a carrier, which brings several

Abbreviations: APR, Aqueous phase reforming; DFAFC, Direct formic acid fuel cell; FA, Formic acid; GC, Gas chromatography; HPLC, High-pressure liquid chromatography; HWE, Hot water extraction; IUPAC, International Union of Pure and Applied Chemistry; PFD, Process flow diagram; rds, Rate determining step; RID, Refractive index detector; TCD, Thermal conductivity detector; TEM, Transmission electron microscopy; WGS, Water-gas shift reaction; OxFA, Oxidation to formic acid.

* Corresponding author.

https://doi.org/10.1016/j.cattod.2021.10.022
Received 26 June 2021; Received in revised form 5 October 2021; Accepted 26 October 2021
Available online 28 October 2021

Nomenclature

Latin letters

c	Concentration, mol/m^3
D	Diffusion coefficient, m^2/s
K	Equilibrium constant, u.u.
k	Reaction rate constant, 1/s
M	Molar mass, g/mol
$\dot{m}$	Mass flow, g/s
$\dot{n}$	Flow of amount of substance, mol/s
p	Pressure, Pa
R^2	Degree of explanation, %
r	Reaction rate, mol/g/s
Re	Reynolds number, -
S	Surface area, m^2/g
T	Absolute temperature, K
V	Volume, m^3
$\dot{V}$	Volumetric flow rate, m^3/s
X	Conversion, %
x	Amount of substance fraction, mol/mol
Y	Yield, %
y	Partial pressure ratio, %
z	Dimensionless length coordinate, -

Greek letters

η	Dynamic viscosity, Pa·s
ν	Flow velocity, m/s
ξ	Extent of reaction, -
ρ	Density, g/cm^3
τ	Residence time, s
τ	Tortuosity, -
φ	Volume fraction, l/l; %
ω	Mass fraction, g/g; %

Constants

R	Gas constant, 8.3143 J/(K·mol)

Subscripts and superscripts

A	HCOOH, formic acid
B	Bed
C	CO_2
c	concentration
cat	catalyst
D	Dimer
e	Effective
F	HCOO, formate
FA	Formic acid, HCOOH
H	H_2
K	Knudsen
M	Monomer
m	Molecular
P	Particle
p	Pressure
R	Reaction
tot	Total
*	Active site

advantages and makes handling much easier. It is liquid under mild conditions, it as low toxicity and low flammability [1]. Hence, FA can be used as a storage medium for both mobile and stationary applications.

FA is supposed to be an alternative fuel for automotive and mobile applications. Direct formic acid fuel cells (DFAFC) are becoming increasingly popular, leading to a growing interest of several research groups [7]. The volumetric energy density of FA can exceed the one of pressurised hydrogen, which makes it an attractive fuel for vehicles. Moreover, DFAFCs can be used as power sources in very small devices. The improvement of currently available batteries is limited and will not be able to meet the increasing demand. For this reason, it is conceivable that mobile applications, such as laptops or smartphones, could be equipped with DFAFCs [7]. The drawback of formic acid is its corrosive properties, which put special demands on the material solutions in the storage and use.

FA plays an important role in the field of biorefining and green chemistry. The transition from oil-based to bio-based production of chemical compounds is increasingly focused by industrial companies. Both oil- and bio-based feedstock must be pre-treated before using them for the production of chemicals. In contrast to fossil resources, natural resources are subject to variations due to environmental fluctuations, which makes it much more complex to extract the desired ingredients from biomass. Renewable resources, such as sawdust and grains, are considered to be suitable feedstock for hydrocarbons [8]. FA might become one of the important key components in C1 chemistry, because FA can be used as a homogeneous catalyst for the hot water extraction (HWE) of hemicelluloses from biomass. The hydrolysis of hemicelluloses to sugar oligomers and monomers is significantly influenced by the acidity of the solution [9]. The hydrolysis process brings out an aqueous solution, which still contains a certain amount of FA. Aqueous phase reforming (APR) can be a subsequent step to produce hydrogen or hydrocarbons from sugars. Simultaneously with the reaction of the sugars to hydrocarbons in APR, FA decomposes to hydrogen and carbon dioxide. FA can improve the selectivity to hydrogen in this process [10]. In conclusion, this is an additional way of sustainable hydrogen production.

1.2. Formic acid decomposition

In order to use formic acid efficiently in new and innovative processes, it is necessary to understand the decomposition of FA. Surprisingly, very little has been published so far on the detailed kinetics of FA decomposition in gas phase [11–15]. Two principal routes of FA decomposition exist, as displayed below,

$$HCOOH \rightarrow CO_2 + H_2 \text{ (I) } \Delta G = -48{\cdot}4 \text{ kJ/mol}$$

$$HCOOH \rightarrow CO + H_2O \text{ (II) } \Delta G = -28{\cdot}5 \text{ kJ/mol}$$

The first reaction is exothermic dehydrogenation, where FA reacts to carbon dioxide and hydrogen. Endothermic dehydration is the second route, where the products are carbon monoxide and water. The ratio between the two pathways depends on the reaction conditions and the presence of a catalyst. Dehydrogenation should be the preferred reaction for two reasons. On the one hand, the desired product is hydrogen. On the other hand, formation of carbon monoxide should be avoided, due to its behaviour as a catalyst poison. Typical heterogeneous catalysts which have been used for the FA decomposition are Pt, Pd, and Ni. In the present work, Pd was used because it had shown a high activity in APR of sugar alcohols [10] in the presence of FA.

The main aim of this work was to conduct kinetic experiments in laboratory scale and interpret the results. The experimental data were obtained through the usage of a fixed bed reactor with a supported palladium catalyst. Different process parameters were varied and their impact on the reaction kinetics were investigated. A mathematical model was supplied with the experimental data.

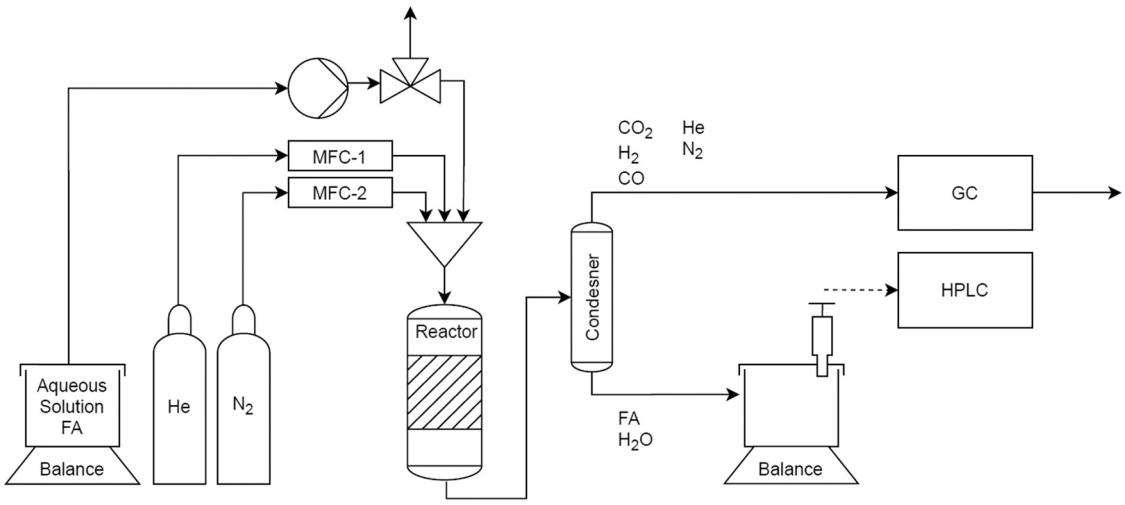

Fig. 1. Process flow diagram of the experimental setup for FA decomposition.

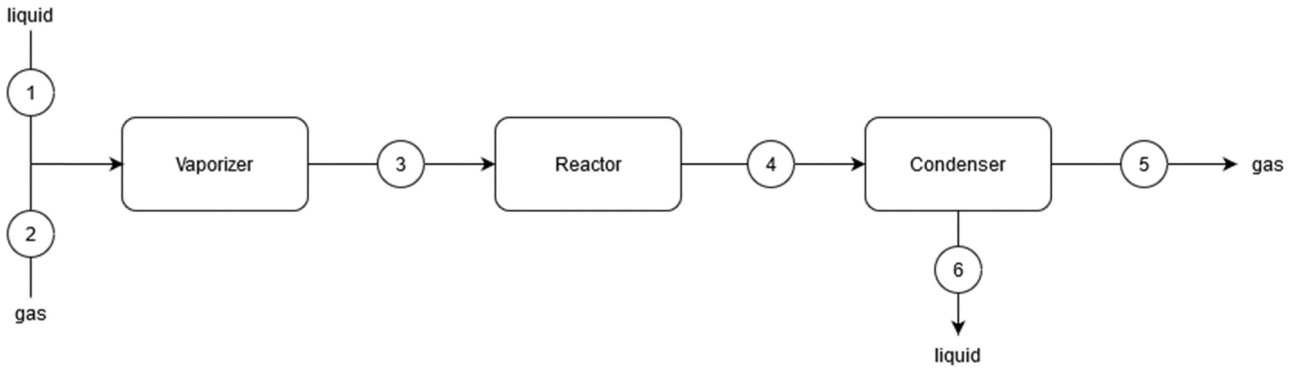

Fig. 2. Block diagram for calculations of the process steps.

2. Experimental section

2.1. Reactor system

The kinetic experiments were performed in a laboratory-scale fixed bed, which was operated in downflow mode. Fig. 1 shows the process flow diagram (PFD) of the experimental setup.

The reactor tube was made of stainless steel with a diameter of 10 mm and a length of about 400 mm. The catalytic fixed bed in the middle of the tube had a length of approximately 40 mm. The reactor was equipped with a heating jacket and a thermal controller (Carbolite Furnaces) to adjust the reaction temperature. By measuring the temperature inside the fixed bed, a thermocouple gave the input signal for the temperature control. Isothermal conditions in the reactor were confirmed by these measurements. The inert part of the tubular reactor was filled with quartz sand. For the fixed bed, a layered mixture of catalyst and quartz sand was used.

2.2. Catalyst and catalyst bed

A palladium catalyst supported on active carbon (Pd/C, 1 wt% Pd) was selected for the decomposition experiments of FA. The carbon support had a mesoporous structure with the commercial trademark Sibunit. The catalyst was manufactured and activated at the Boreskov Institute of Catalysis in Novosibirsk. Palladium was chosen for the active material, because of its high selectivity for the favoured decomposition pathway and a low susceptibility for poisoning.

The tubular reactor was mainly filled with quartz sand as an inert material. The packed catalyst bed was inserted in several layers, each consisting of about 10 particles. The catalyst had particle sizes 1.6–2.0 mm. To fill the interstices, every layer was covered with quartz sand. The number of layers was dependent on the total mass of the catalyst, which was changed in different experiments. It was not possible to create a homogeneous mixture of quartz sand and catalyst before filling the reactor. Due to the high porosity of the catalyst particles, they separated from the inert material, so that two separated fractions were formed. Besides, the layered structure of the fixed bed prevented bypass flow and the appearance of dead zones. The catalyst amount was 0.1 g. The liquid flow consisting of an aqueous solution of formic acid at the reactor inlet was typically 0.64 g/min and the gas flow consisting of helium and nitrogen was 200 ml/min at 25 °C. In the vaporizer placed in front of the reactor tube the liquid flow was vaporized and mixed with the gas flow. Thus the only gas entered the reactor tube.

2.3. Experimental steps

All the experiments followed the same procedure with several steps. At the beginning of the experiment, the reactor was flushed with helium as the inert gas. The flow rates were adjusted with a fraction of 97% helium and 3% nitrogen. Before starting the experiment, two gas-phase samples were analysed by gas chromatography (GC) to ensure a constant gas composition and prevent impurities. The GC analysis was started and the injection of the aqueous FA feed solution was done with a certain time offset depending on the series of experiments. The product analysis was carried out by means of auto sampling GC and manual sampling HPLC (Section 2.5). After finishing the experiment, the reactor was

flushed again with inert gas to ensure that no FA was left in the reactor. The catalytic experiments were carried out at 150–225 °C to minimize the impact of self-decomposition of formic acid.

2.4. Calculations

FA was inserted as a liquid feed solution, vaporized in before entering the reactor, decomposed in the reactor and some components were condensed after the reaction. Based on Fig. 1, a schematic diagram displayed in Fig. 2 was created to illustrate the calculations at the different units of the device.

To compare the experimental results, the conversion of FA was used as a quantitative descriptor. For the present reactor system with point 3 in Fig. 2 as the reactor inlet and point 4 as the reactor outlet, the conversion is defined as

$$X_{FA} = \frac{\dot{n}_{3,FA} - \dot{n}_{4,FA}}{\dot{n}_{3,FA}} \quad (1)$$

2.4.1. Inlet molar flow of formic acid

The inlet molar flow of FA can be calculated from the inserted mass flow of FA at point 1,

$$\dot{n}_{3,FA} = \dot{n}_{1,FA} = \frac{\dot{m}_{1,FA}}{M_{FA}} \quad (2)$$

With the given values of the feed concentration and mass flow of the total aqueous feed solution, the FA mass flow is obtained from

$$\dot{m}_{1,FA} = \dot{m}_{1,tot} \bullet \omega_{1,\mathrm{FA}} \quad (3)$$

where ω denotes the mass fraction of FA.

2.4.2. Outlet molar flow of formic acid

Two different approaches were used for the determination of the molar outlet flow of FA. Both, the gas-phase composition at point 5 and the condensed liquid-phase at point 6 were analysed.

2.4.3. Gas-phase analysis

For the parallel reactions of dehydrogenation (I) and dehydration (II), the molar balances are defined as

$$\dot{n}_{4,FA} = \dot{n}_{3,FA} - \xi_I - \xi_{II} \quad (4)$$

$$\dot{n}_{4,CO_2} = n_{4,H_2} = +\xi_I \quad (5)$$

$$\dot{n}_{4,CO} = \dot{n}_{4,H_2O} = +\xi_{II} \quad (6)$$

where ξ is the extent of the reaction. For virtually all the performed experiments, the amount of carbon monoxide was very low with a selectivity of 1–2% only. Therefore, the dehydration reaction (II) is neglected in the following calculations.

According to the overall stoichiometry, the amounts of carbon dioxide and hydrogen should be equal. Thus, both components could be used to add to the molar balance, if the ratio would be 1:1. This was however not exactly observed in all the experimental results. Consequently, the average amount of both components was used to diminish the fluctuations in the analysis.

Because of the low pressure, the ideal gas law was used in the calculations. The justification of using the ideal gas law was confirmed by estimating the compressibility factor of the gas mixture. The factor was very close to 1. The whole reactor system was working under atmospheric pressure and the pressure drop inside the reactor was negligible. The molar flows of the product components were determined from the GC analysis after the condenser at point 5,

$$\dot{n}_{4,CO_2} = \dot{n}_{5,CO_2} = \frac{p \bullet \dot{V}_{5,CO_2}}{R \bullet T_5} \quad (7)$$

The volumetric flow of carbon dioxide is calculated based on the total volumetric flow and the volume fraction,

$$\dot{V}_{5,CO_2} = \dot{V}_{5,tot} \bullet \varphi_{5,\mathrm{CO_2}} \quad (8)$$

To quantify the total volumetric flow rate, a constant nitrogen flow was used as an internal standard. The volumetric nitrogen flow is constant from point 2 to point 5 in Fig. 2, while the volume fraction changes because of the reaction. The volume fraction of nitrogen is proportional to the total volumetric flow.

$$\dot{V}_{5,tot} = \dot{V}_{2,tot} \bullet \frac{\varphi_{2,\mathrm{N_2}}}{\varphi_{5,\mathrm{N_2}}} \quad (9)$$

The volume fractions of all the gas-phase components were determined by the gas chromatographic analysis. The volume fraction is proportional to the peak area in the chromatogram,

$$\varphi_{5,N_2} = \varphi_{5,N_2,cal} \bullet \frac{\mathrm{A_{N_2}}}{\mathrm{A_{N_2,cal}}} \quad (10)$$

where 'cal' refers to the calibration peak in the GC analysis.

2.4.4. Liquid-phase analysis

The second approach to quantify the molar outlet flow of FA is to measure the non-reacted amount of FA in the liquid phase. The analysis was performed by HPLC. The molar outlet flow at point 4 is equal to the molar flow at point 6 and the molar flow can be calculated from the mass flow,

$$\dot{n}_{4,FA} = \dot{n}_{6,FA} = \frac{\dot{m}_{6,FA}}{M_{FA}} \quad (11)$$

To calculate the mass flow of FA, the mass fraction obtained from HPLC was used,

$$\dot{m}_{6,FA} = \dot{m}_{6,tot} \bullet \omega_{6,\mathrm{FA}} \quad (12)$$

2.5. Gas and liquid chromatography

Gas chromatography (GC) was used to analyse the product composition in the gas phase. The analysis device was an Agilent Technologies 680 N GC equipped with capillary columns and a thermal conductivity detector (TCD). The carrier gas was helium with a total volumetric flow of 46.6 ml/min. Two consecutive capillary columns with the lengths of 30 m and diameters of 530 μm were used. The first column (HP-PLOT Q) had a film thickness of 40 μm, while the second one (HP-MOLSIV 5 A) had a film thickness of 25 μm. The GC operated isothermally at 15 bar and 70 °C. To quantify the concentrations, nitrogen was used as the calibration gas. Nitrogen with a volume fraction of 3% was added to the helium carrier gas as an internal standard- Not all of the components, which were present in the gas phase after the reactor outlet, could be analysed in the GC. Hence, the molecules with high boiling points were separated in a condenser before the GC. Consequently, four gas components were analysed. Hydrogen is the only analysed molecule, which has a higher thermal conductivity than helium. To obtain positive peaks for all components, the polarity of the column was inverted in the retention time range from 3.5 to 4.2 min

The FA concentration in the reactor outlet was analysed by high-pressure liquid chromatography (HPLC). The device was Agilent Technologies 1100 series HPLC. A sulphuric acid solution with a concentration of 0.005 mol/l was used as an eluent with a flow rate of 0.6 ml/min. The device was equipped with an Aminex HPX-87 H column, which had a length of 300 mm and a diameter of 7.8 mm. It operated at 45 °C and 80 bar. To analyse the component responses, a refractive index detector (RID) was used. A series of samples with known concentrations were used for the calibration. With the linear plot of the concentration as a function of the peak areas, it was possible to extract calibration curves and calculate the unknown sample concentrations.

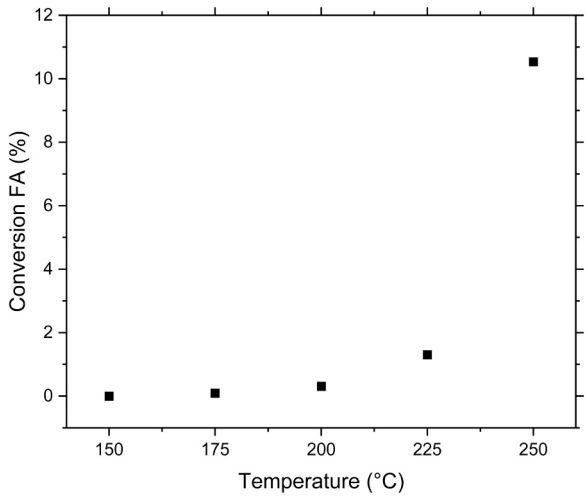

Fig. 3. Influence of the reaction temperature on the thermal decomposition of formic acid.

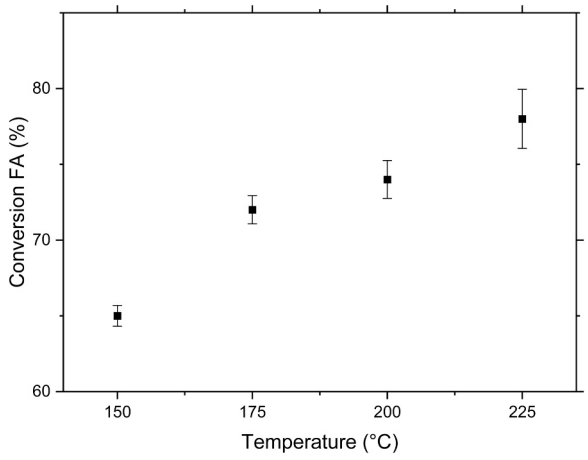

Fig. 4. Influence of the reaction temperature on the catalytic decomposition of formic acid.

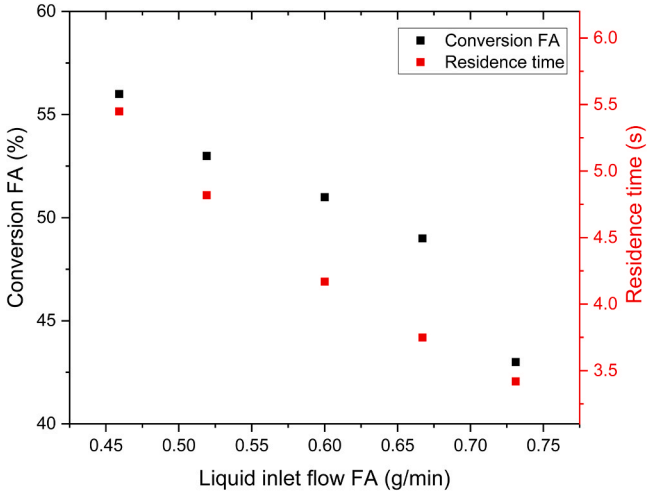

Fig. 5. Influence of the flow rate on the catalytic decomposition of formic acid.

3. Experimental results and discussion

3.1. Thermal decomposition of formic acid

The first step of the experimental work was to investigate the thermal decomposition of FA in the absence of catalysts. In order to examine the reaction kinetics of the catalytic decomposition, thermal decomposition should be avoided. In this way, it can be ensured that only the presence of the heterogeneous catalyst is exclusively responsible for the decomposition. The idea was to find a suitable temperature range, where the impact of thermal decomposition can be neglected.

According to literature, thermal decomposition is anticipated at 200 – 250 °C [1]. Therefore, the experimental investigation was carried out at five temperatures within the interval 150 – 250 °C. The mass flow of the aqueous feed solution was set to 0.16 g/min with a FA mass fraction of 7%. The volumetric flow of the inert gas was set to 50 ml/min.

Fig. 3 displays the conversion of FA as a function of the reaction temperature. The thermal decomposition increases exponentially rising reaction temperature. Within the temperature range of 150 – 200 °C the conversion of FA remained below 1%. The increase of the thermal decomposition starts at 225 °C with a conversion of 1.3%. At 250 °C the conversion increases to 10.5%. In practice, conversions below 2% can be neglected in the quantitative treatment of the kinetic data. Hence, the reaction temperature range for the catalytic decomposition was set to 150 – 225 °C.

3.2. Influence of the main process parameters

The influence of the main process parameters was investigated in third steps. An overview of the experimental conditions is displayed in Appendix I. For the following diagrams of the experimental results, the average steady state values were used. The long-term stability is discussed in Section 3.3.1.

3.3. Influence of the reaction temperature

As the first main process parameter, the influence of the reaction temperature on the reactant conversion and product selectivity was investigated by systematic experiments. The decomposition of FA was carried out at 150, 175, 200 and 225 °C. The experimental results are displayed in Fig. 4.

Fig. 4 shows the increasing conversion of FA at different reaction temperatures. The values reflect the average conversion during the stationary state of the reaction system with the related standard deviations, which were typically less than 5%. As expected, the trend shows an increase of the FA conversion with a rising temperature. The conversion increases from a minimum of 65% at 150 °C to a maximum of 78% at 250 °C and the standard deviation of the measurements increases at higher temperatures.

Besides the reaction kinetics, the thermodynamics is affected by temperature. The dominant dehydrogenation reaction (I) is slightly exothermic. Hence, the equilibrium is shifted to the side of the reactants by increasing the temperature. The dehydration is slightly endothermic, so that this reaction behaves in the opposite way [13]. The formation of carbon monoxide and water is promoted at increasing temperature. Therefore, the ratio of dehydrogenation to dehydration and the selectivity changes accordingly. The selectivity of hydrogen decreases from 99% at 150 °C to 97% at 250 °C.

3.3.1. Influence of the flow rate

The second set of systematic experiments was focused on the variation of the liquid flow rate. Both the liquid and the gas inlet flows were changed proportionally, so that the ratio between all the components was kept constant. This enables investigating, how the flow rate affects the reactant residence time and the reactant conversion. Fig. 5 displays the experimental results of the influence of the flow rate as a main

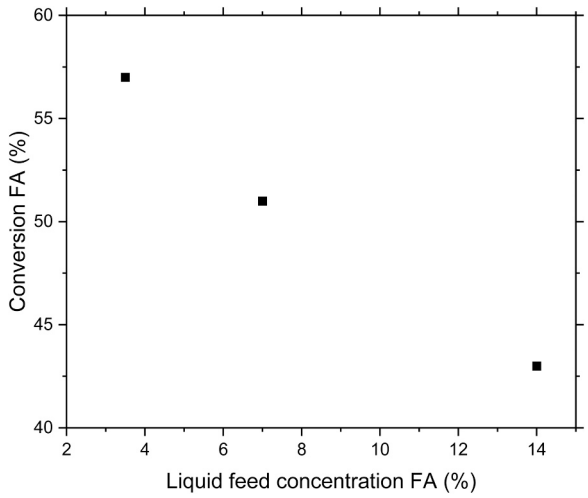

Fig. 6. Influence of the feed concentration on the catalytic decomposition of formic acid.

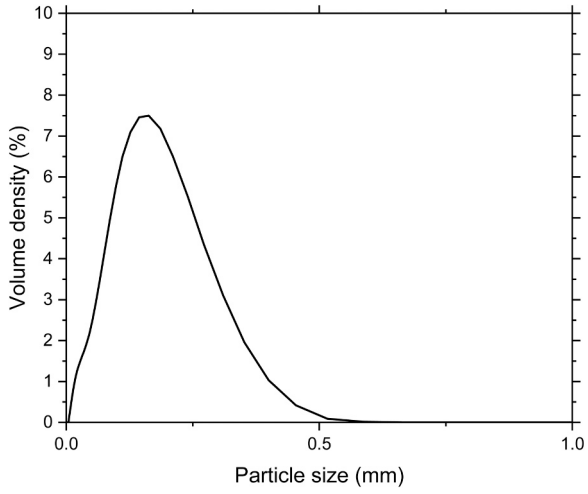

Fig. 7. Particle size distribution of the crushed catalyst.

process parameter.

The residence time τ is defined for systems with constant gas flow rates $\tau = \frac{V_R}{\dot{V}}$,

where V_R is the reaction volume and $\dot{V}$ is the volumetric flow rate. Detailed calculations are reported in Appendix II. The residence time varied from 5.45 s with the lowest flow rate 0.46 g/min to 3.42 s with the highest flow rate 0.73 g/min. The residence time had a decisive influence on the conversion of FA. The conversion varied from 56% with the lowest flow rate 0.46 g/min to 43% with the highest flow rate 0.73 g/min. The diminished possibility of interaction between the reactant and the active sites on the catalyst surface at higher flow rates causes a decrease of the conversion.

3.3.2. *Influence of the FA, H_2 and CO_2 concentrations*

The liquid feed concentration of FA is another important process parameter, which influences the reactant conversion. The catalytic decomposition was carried out with three different mass fractions of FA, 3.5%, 7% and 14%. The overall flow rates of the liquid feed solution and the carrier gas were kept constant. Thus, the ratio between FA and the other components was changed.

The conversion of FA as a function of the liquid feed concentration of FA is shown in Fig. 6. With the reference mass fraction of 7%, the conversion of FA was 51%. The dilution of the liquid feed solution to 3.5% of FA caused an increase of the conversion to 57%. Beyond this, the mass fraction was increased to 14%, which led to a conversion of 43%. The plot shows a distinct trend: the higher the liquid feed concentration, the lower is the reactant conversion. The different degrees of dilution change the ratio between FA as the reactant and all other components, which are present in the reactor inlet mixture. Thus, with a higher liquid feed concentration more FA is injected into the reactor. Even if in this way the amount of formed product increases, the ratio between reacted and unreacted FA decreases, which leads to a lower reactant conversion.

Few additional experiments were carried out to investigate the effect of the products, hydrogen and carbon dioxide on the reaction kinetics. Hydrogen or carbon dioxide was added to the feed and the results were compared with those obtained with FA and inert gas feed. It could be expected that adsorption of H_2 and CO_2 would retard the FA decomposition rate. However, such effect was not detected in our experiments indicating that the product adsorption is weak compared to the FA adsorption on the catalyst surface.

3.3.3. *Influence of hydrogen pre-treatment*

To get more information about the palladium catalyst, experiments with additional pretreatment steps were carried out. Before the start of the catalytic decomposition experiment, the catalyst bed was flushed with hydrogen. After flushing the reactor at room temperature with inert gas as the first experimental step, the gas flow was changed to pure hydrogen with a flow rate of 50 ml/min. The reactor was heated up to 250 °C with rate of 5 °C/min. Under a constant temperature of 250 °C the catalyst bed was flushed with hydrogen for 1 h. After the pre-treatment, the reactor was cooled down to reaction temperature and the normal experimental procedure was commenced.

At 175 °C the experiment with the pre-treatment of hydrogen gave a reactant conversion of 71%, whereas the reference experiment without pre-treatment showed a reactant conversion of 73%. The difference in the FA conversion was very minor and consequently, the pre-treatment with hydrogen caused no significant improvement of the subsequent catalytic decomposition of FA. This observation supports the hypothesis that the active sites of Pd were permanently in a reduced state in the experiments.

3.3.4. *Influence of the catalyst particle size*

The influence of the particle size on the catalytic decomposition of FA was investigated to reveal the role of internal mass transfer resistance in the catalyst pores. For that purpose, two experiments were conducted out with the same catalyst batch, but with different particle sizes. First a reference experiment with a new batch of catalyst and the reference process parameters was performed. After that, the catalyst was taken out of the reactor tube and crushed in a mortar. Thus, the particle size was diminished to 0.004 – 0.6 mm. After crushing the particles, the fixed bed was prepared again with the same procedure as in all other experiments. A laser diffraction equipment, Mastersizer 3000 was used for measuring the macroscopic particle size distributions of the crushed catalyst. A detailed analysis of the particle size distribution is displayed in Fig. 7. The original catalyst particles showed the same activity as the crushed ones, thus indication the operation in the regime of kinetic control and the absence of diffusion limitations inside the catalyst particles.

The particle size distribution shows a peak at 0.163 mm. The FA conversion of the experiment with the crushed catalyst particles was 63%. Before crushing the particles, the same batch was used uncrushed for a reference experiment, giving the FA conversion 75%. The conversion with crushed particles was 12% lower than the one obtained with uncrushed particles. The catalyst particle size can influence the reactant conversion due to two phenomena. The smaller the particles, the shorter is the diffusion distance to the active sites, which should increase the overall reaction rate. However, this assumption, that a smaller particle size improves the conversion was not confirmed. Consequently, the reaction was presumed to not to be diffusion limited.

Possible reasons for the lower conversion of the experiment with

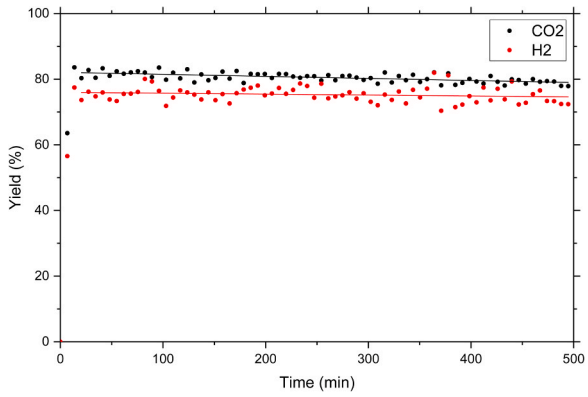

Fig. 8. Results of catalyst stability test – yield vs time-on-stream.

Table 1
Linear fit parameters for the stability test of the catalyst.

	Intercept [%]	Slope [%/min]	Y_{Min} [%]	Y_{Max} [%]	ΔY [%]
CO_2	82	-0.006	78	84	6
H_2	76	-0.002	70	82	12

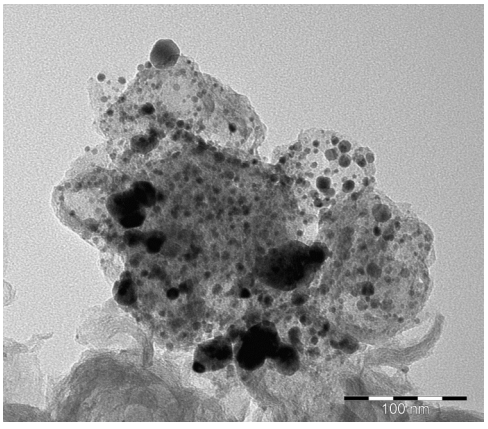

Fig. 9. TEM analysis of the palladium clusters.

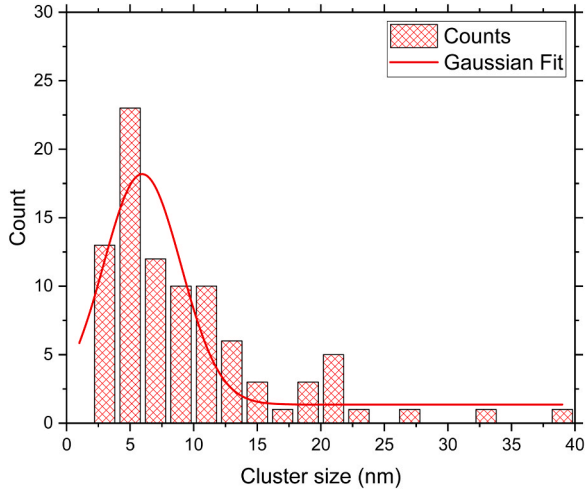

Fig. 10. Palladium cluster size distribution.

crushed particles could be found in the preparation of the fixed bed. The same mass of catalyst was weighted before the preparation, but for the crushed particles a loss of mass was conceivable. The catalyst mass has a crucial influence on the reactant conversion, so that the uncertainty in the fixed bed preparation could be an explanation for the lower conversion. Besides, some small particles were found on the lower part of the reactor tube when removing the catalyst bed and the quartz sand. This leads to the assumption that a certain amount of the crushed particles was flushed out of the reactor tube.

The role of external mass transfer resistance was checked by evaluation the Sherwood and Biot numbers. The diffusion coefficient and Reynolds number calculations are reported in Appendices IV-V. By using the correlation which relates the Sherwood number to Schmidt and Reynolds numbers, the order of magnitude of Sherwood number was estimated to 13, which gives the Biot number 13 for the lowest possible value of the particle tortuosity (=1). However, with a high probability the tortuosity is clearly higher than 1, which means that the Biot number $>>13$, indicating that external mass transfer resistance does not affect the catalyst effectiveness factor.

3.4. Catalyst characterisation and durability

The formic acid conversion and the hydrogen selectivity of the reaction system were decisively influenced by the Pd/C catalyst. Therefore, the investigation of the catalyst properties was important. The catalyst stability was examined in long-term experiments and a TEM analysis gave insights in the cluster size distribution of palladium.

3.4.1. Long-term stability

The stability of the heterogeneous catalyst is an important aspect to evaluate experimental results in laboratory scale and particularly for the application in industrial scale. The results of a stability test are shown in Fig. 8. The conversion level changed slightly within the experiments despite constant process parameters. This led to the hypothesis that the catalyst deactivated during the experiments and therefore it was necessary to investigate the long-term stability. The fixed bed reactor was loaded with a new batch of catalyst and the experiment was carried out over 8 h.

Fig. 8 shows the yields of the main product components CO_2 and H_2 and the linear fits at the steady state. Both graphs fluctuate slightly due to measurement uncertainties. It is noticeable that the fluctuation for the carbon dioxide curve is significantly lower than the one for hydrogen, which is explained with the different sensitivities of the components in the GC analysis. The GC signal peak for carbon dioxide was much higher than for hydrogen due to the very different response factors of these components.

Both linear fits in Fig. 8 showed slightly negative slopes. Over the experiment duration of 8 h, the average conversion for carbon dioxide and hydrogen decreased by 3% and 1.4%, respectively. The parameters of the linear fits are displayed in Table 1.

A special series of successive experiments was conducted by starting the process with a clean catalyst surface, exposing it to the reactive mixture, continuing the experiment for few hours, switching to inert gas flow until the concentrations of the reactive components became zero. This cycle was repeated four times. The conditions were T = 150 °C, FA flow 0.8 ml/min and inert gas flow 200 ml/min. The inlet FA concentration was 1.12% in molar fraction. The steady state conversion of FA was 31%, 28%, 30% and 33% in the successive experiments and the molar ratio CO_2-to-H_2 was one in the experiments. In general, the catalyst can be considered to be stable and no irreversible deactivation was figured out. Besides, the long-term stability led to the conclusion that the uncertainties in all the systematic experiments were caused by minor fluctuations in the GC analysis. Therefore, the average steady state values comprising several experimental points at the end of the experiment were used for the calculation of the conversion of formic acid.

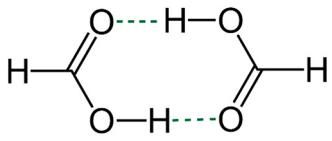

Fig. 11. Skeletal formula of a cyclic FA dimer.

Table 2
Modelling results for three different rate equations for FA decomposition.

Parameter Error (%)	Simple adsorption mechanism $r = \frac{k' \cdot c_A}{1 + K_A \cdot c_A}$	Adsorption-dissociation mechanism $r = \frac{k' \cdot c_A}{(1 + K_A \cdot c_A)^2}$	1st order $r = k' \cdot c_A$
k′ [1/s]	0.39 2.3%	0.359 3.2%	0.23 3.9%
E_a [J/mol]	$1.80 \cdot 10^4$ 10%	$1.84 \cdot 10^4$ 8.1%	$2.68 \cdot 10^4$ 9.2%
K_A [m^3/mol]	1.52 5%	0.52 6.3%	–
R [%]	90.2	90.5	80.1

T_{mean}= 448 K (175 °C)

Table 3
Correlation matrix for the adsorption-dissociation model.

k_1	1.000	
E_{a1}	0.233	1.000
K_A	0.694	− 0.210 1.000

3.4.2. *Distribution of palladium nanoparticles*

The palladium nanoparticles on the carbon support were investigated with high-resolution transmission electron microscopy (HR-TEM). The analysis device was a JOEL JEM-1400 Plus in the Laboratory of Electron Microscopy at the University of Turku. With a resolution of up to 0.38 nm, the palladium clusters in 1% Pd/C used in the kinetic experiments were investigated. A TEM image is displayed in Fig. 9.

The palladium clusters are visible with a higher contrast (dark grey/black) supported on the mesoporous active carbon structure (light grey). The majority of the palladium clusters are very well dispersed. Only few clusters are accumulated to larger ones. To investigate the cluster size distribution, the diameters of 90 clusters from five different positions were determined. The histogram is displayed in Fig. 10.

The diagram shows the counts of clusters over the cluster diameter. Additionally, the modified Gaussian fit was implemented by using the Origin software. At lower diameters, the highest frequency is observed for particle diameters 5–6 nm. Few clusters show larger diameters up to 39 nm. It is possible, that these larger clusters were formed by sintering during the experiments.

4. Kinetic and reactor modelling

The experimental data obtained from the laboratory scale fixed bed reactor were utilised for the mathematical modelling of the current

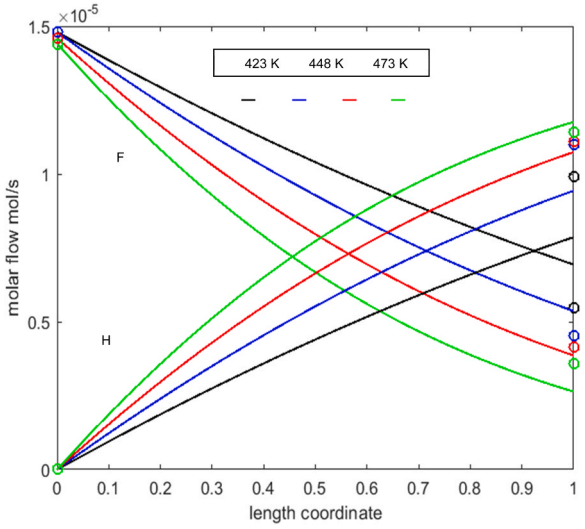

Fig. 13. Molar flow profiles for different reaction temperatures.

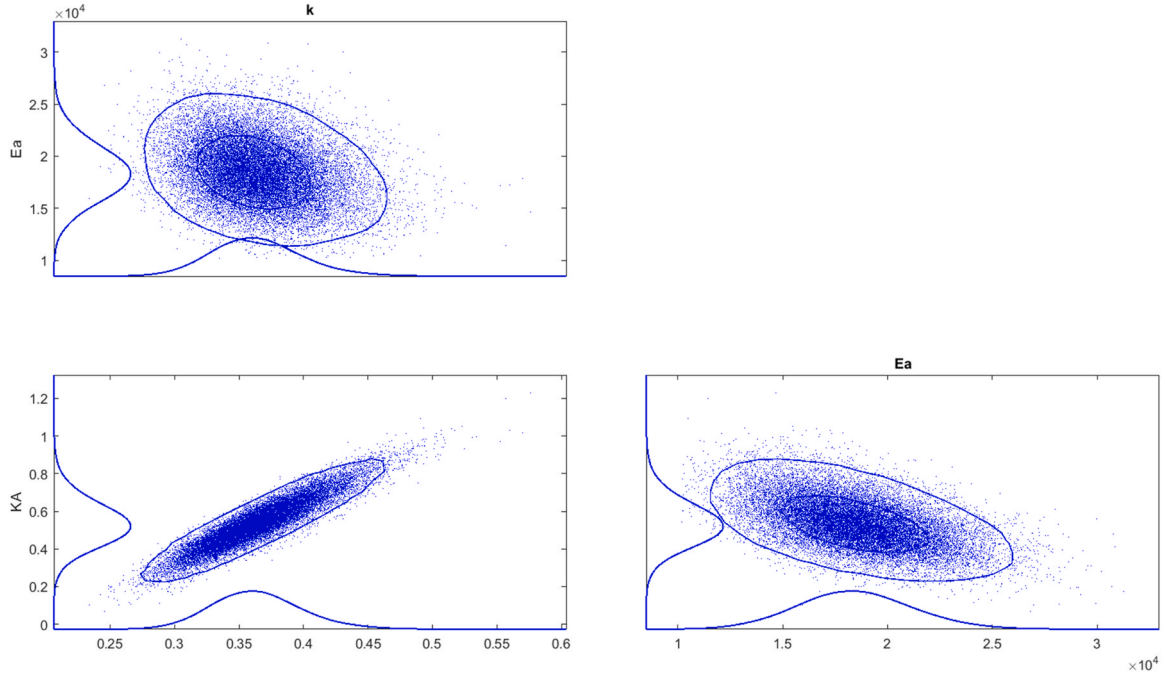

Fig. 12. MCMC diagram for the adsorption-dissociation model.

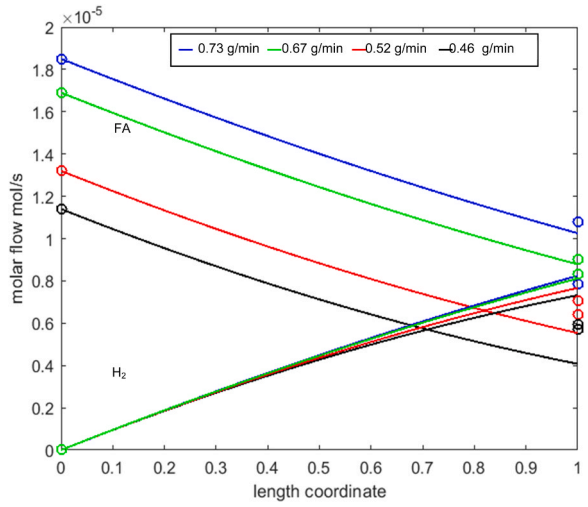

Fig. 14. Molar flow profiles for different flow rates.

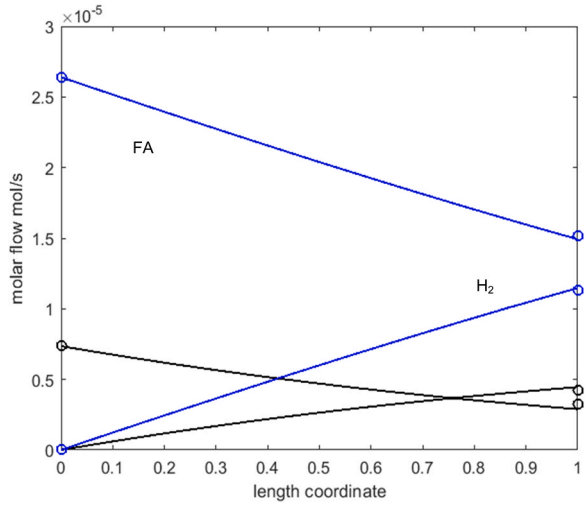

Fig. 15. Molar flow profiles for different feed concentrations.

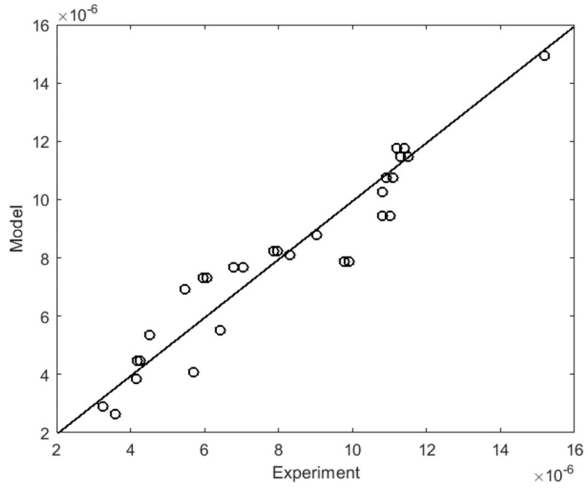

Fig. 16. Parity plot for the adsorption-dissociation model. FA, H_2 and CO_2 concentrations included.

reaction system. The investigation of the reaction kinetics is a helpful tool to determine the reaction mechanism for the decomposition of FA. The calculations presented here give the basis for mathematical modelling.

4.1. Dimerisation of formic acid

A certain amount of FA dimerises in liquid and gas phases, where monomers of FA are coupled to each other by hydrogen bonds. Fig. 11 shows the structure of a FA dimer.

Hydrogen bonds (marked with —) are formed between the molecules, so that a cyclic dimer is formed. Depending on the conditions, the dimerised form of FA is more favoured than single molecules. Therefore, FA deviates in its behaviour sometimes from an ideal gas [1,16,17]. The formation of the dimerised form occurs primarily at lower temperatures. The gasphase consists of 95% cyclic FA dimers at room temperature and atmospheric pressure [17]. Therefore it could be suspected that a certain fraction of FA forms dimers in gas phase, which might have an impact on the reaction kinetics. The amount of FA monomers was calculated to assess the relevance of FA dimerisation for the kinetic and reactor modelling. A detailed description of the mathematical treatment can be found in Appendix III.

The equilibrium between monomers and dimers can de facto be considered as a chemical reaction,

$$2\,M \leftrightarrow D$$

To quantify the amount of monomers under the actual reaction conditions, a new parameter y is defined, expressing the ratio between the partial pressure of the remaining monomers after the dimerization reaction and the initial monomer partial pressure,

$$y = \frac{p_M}{p_{0,M}} \tag{13}$$

Equilibrium prevails in the gas phase, where the ideal gas law can be applied separately for the monomers and dimers. Therefore, the equilibrium constant can be expressed with the partial pressures,

$$K_p = \frac{p_D}{{p_M}^2} \tag{14}$$

Prausnitz and Gmehling [16] have reported the values for the calculation of the pressure based equilibrium constant for formic acid dimerisation,

$$-\log K_p[torr^{-1}] = 10.743 - \frac{3083}{T} \tag{15}$$

The parameter y was calculated with the reaction conditions, giving the lowest amount of FA monomers.

At least 97.7% of FA are monomers in gas phase at 150 °C and with a FA concentration of 14 wt%. The fraction of monomers is even higher, as the reaction conditions are shifted to higher temperatures and lower concentrations. The amount of FA dimers under the reaction conditions is vanishingly small in our kinetic experiments. Consequently, the dimerisation of FA can be neglected in the mathematical modelling of the process under the actual circumstances.

4.2. Diffusion effects

In order to evaluate the role of internal mass transfer resistance in the pores of the catalyst particles, the diffusion coefficients of the components were estimated from available correlations. According to the mean transport pore model, the effective diffusion coefficient is obtained from the molecular diffusion coefficient as follows [18],

$$D_{ei} = \frac{\varepsilon_P}{\tau_P} \bullet \mathrm{D_i} \tag{16}$$

where ε_P is the particle porosity and τ_P is the labyrinth factor, i.e. the

particle tortuosity. In fact, the diffusion coefficient of a certain gas-phase component consists of the contributions of intermolecular collisions and collisions between the molecules and the pore walls. The latter effect is called Knudsen diffusion. The combined diffusion coefficient can be obtained from

$$D_i = \frac{1}{\frac{1}{D_{mi}} + \frac{1}{D_{Ki}}} \tag{17}$$

where the individual molecular diffusion coefficient is calculated from the molar fractions and the binary molecular diffusion coefficients, according to the Wilke approximation,

$$D_{mi} = \frac{1 - x_i}{\sum_{k=1, k\neq i}^{N} \frac{x_k}{D_{ik}}} \tag{18}$$

The binary molecular diffusion coefficients are related to the interactions between each pair of the gas-phase components; the Fuller-Schettler-Giddings equation is used [18],

$$\frac{D_{ik} = T^{1.75} \bullet \left(\frac{1}{M_i} + \frac{1}{M_k}\right)^{\frac{1}{2}} \bullet 10^{-7}}{p \bullet \left(v_i^{\frac{1}{3}} + v_k^{\frac{1}{3}}\right)^2} \tag{19}$$

and for the Knudsen diffusion coefficient is valid,.

$$D_{Ki} = \frac{8\varepsilon_P}{3 S_g \rho_P} \sqrt{\frac{2RT}{\pi M_i}} \tag{20}$$

The values of diffusion coefficients were estimated at the inlet conditions of the feed using the procedure described above. The calculations are shown in Appendix IV. A comparison of the diffusion coefficients with the experimental rate data suggests that the system operated under kinetic control. Furthermore, the kinetic control was confirmed by comparing the FA conversions obtained with original and crushed catalyst particles (Section 3.2.5).

4.3. Flow pattern and reactor model

The flow regime in the fixed bed was checked by calculating the Reynolds number from the expression

$$\frac{Re = \rho \bullet v \bullet d_{particle}}{\eta} \tag{21}$$

The details of the calculations are given in Appendix V. Under the current reaction conditions, the Reynolds number was estimated to $Re = 13$. This value is within the transitional region for packed beds, but close to the boundary value for laminar flow of $Re < 10$. The flow conditions can be assumed to be laminar and a plug flow model can be used for the reactor modelling, which is defined as

$$\frac{d\dot{n}_i}{dz} = \rho_B V_R r_i \tag{22}$$

Eq. (22) represents a pseudo-homogeneous one-dimensional model for a fixed bed reactor, where neither radial concentration nor temperature gradients appear inside the reactor tube. The molar flow gradients are only dependent on the dimensionless length coordinate z. The catalyst bulk density ρ_B is defined as the ratio of catalyst mass and the total reactor volume,

$$\rho_B = \frac{m_{cat}}{V_R} \tag{23}$$

4.4. Reaction mechanism and rate equations

The derivation of the reaction rate equations is one of the most important steps in developing a mathematical model for a chemical reaction system. Reaction rates are developed based on reaction mechanisms in combination with assumptions, which steps are rate determining or in quasi-equilibrium. Inspired by previous literature [12, 13], two reaction mechanisms were considered in detail.

4.4.1. Simple adsorption mechanism

The first one was a simple mechanism with a historical background, because the decomposition of FA is principally known for many decades. Hence, the very simple two-step reaction mechanism displayed below was extracted from Mars et al. [13].

Reaction I: **HCOOH** + * ↔ **HCOOH***(quasi-equilibrium) (I)

Reaction II: **HCOOH*** → **H_2** + **CO_2** + *(rds) (II)

FA adsorbs on a single active site in the first step, which is rapid and thus in quasi-equilibrium. In the second step, the products are directly formed from the adsorbed FA molecule and released from the surface. This step is assumed to be rate determining step (rds) and the rate equation can thus be formulated as

$$r_{II} = k_{II} \bullet c_{A*} \tag{24}$$

where the subscript A stands for the reactant FA. For the first step in the quasi-equilibrium, the equilibrium constant is defined as

$$K_I = K_A = \frac{c_{A*}}{c_A \bullet c_*} \tag{25}$$

Additionally, a total balance can be formulated for the surface species. The total concentration of active sites c_0 is the sum of the covered active sites c_{A*} and the free active sites $c*$,

$$c_0 = c_{A*} + c_* \tag{26}$$

By combining the reaction rate equation with the equilibrium constant and the active site balance, it can be rearranged to

$$\frac{r_{II} = k_{II} \bullet K_A \bullet c_A \bullet c_0}{1 + K_A \bullet c_A} \tag{27}$$

If the catalyst is assumed to be stable, the total concentration of active sites remains constant. All constants in the numerator can be summarised to a merged parameter k', which leads to the final reaction rate equation for the simple two-step reaction mechanism,

$$r = \frac{k' \bullet c_A}{1 + K_A \bullet c_A} \tag{28}$$

Adsorption-dissociation mechanism.

The second reaction mechanism is based on the assumption of consecutive adsorption and decomposition steps on the Pd surface. The elementary steps can be described as follows,

Reaction I: **HCOOH** + * ↔ **HCOOH***(quasi-equilibrium) (I)

Reaction II: **HCOOH*** + * ↔ **HCOO*** + **H***(rds) (II)

Reaction III: **HCOO*** + * → **COO*** + **H***(rds) (III)

Reaction IV: **COO*** ↔ **CO_2** + *(quasi-equilibrium) (IV)

Reaction V: **2 H*** ↔ **H_2** + **2***(quasi-equilibrium) (V)

This mechanism is an extension of the mechanism proposed in ref. [12] for FA decomposition on Pt single crystals. The first step is similar to the simple mechanism, where FA adsorbs on the surface. The adsorbed molecule dissociates in two steps, which are rate determining. Step II is assumed to be reversible while step III is assumed to be irreversible. The adsorbed product molecules are released to the gas phase in the last two desorption steps.

For the rate determining steps, the rate equations can be formulated as

$$r_{II} = k_{II}\left(c_{A*} \bullet c_* - \frac{c_{H*} \bullet c_{F*}}{K_{II}}\right) \tag{29}$$

$$r_{III} = k_{III} \bullet c_{F*} \bullet c_{*} \tag{30}$$

where the subscripts H and F refer to hydrogen and the surface intermediate HCOO, respectively. The quasi-steady state hypothesis is applied for the intermediate state HCOO* (F*),

$$r_{F*} = r_{II} - r_{III} \approx 0 \tag{31}$$

The equilibrium constants for steps I, IV and V, as well as the adsorption equilibrium constants are defined as:

$$K_I = K_A = \frac{c_{A*}}{c_A \bullet c_*} \tag{32}$$

$$1/K_{IV} = K_C = \frac{c_{C*}}{c_C \bullet c_*} \tag{33}$$

$$1/K_V = K_H = \frac{{c_{H*}}^2}{c_H \bullet {c_*}^2} \tag{34}$$

where the index C stands for the product CO_2. Additionally, the site balance can be formulated. The total concentration of active sites c_0 is the sum of the covered active sites of the adsorbed components and the vacant active sites c^* ,

$$c_0 = c_{A*} + c_{F*} + c_{C*} + c_{H*} + c_* \tag{35}$$

By combining the reaction rate Eqs. (29)-(30) with the adsorption equilibrium expressions (32)-(34) and the balance of active sites, the rate equation for the adsorption-dissociation mechanism becomes

$$r = \frac{k_{II} k_{III} K_A c_A {c_0}^2}{(\frac{k_{II}}{K_{II}} \sqrt{K_H c_H} + k_{III})(1 + K_A c_A + \sqrt{K_H c_H} + K_C c_C + \frac{k_{II} K_A c_A}{\frac{k_{II}}{K_{II}} \sqrt{K_H c_H} + k_{III}})^2} \tag{36}$$

The details of the derivation of Eq. (36) are provided in Appendix VI. In case that carbon monoxide and water appear in the system, the corresponding adsorption effects should be considered in the model. The rather complex expression can be simplified by making several assumptions for limiting cases. If the desorption steps are rapid, the product components are quickly released to the gas phase and not remain adsorbed on the surface. The experiments reported in Section 3.2.3 indicated that neither hydrogen nor carbon dioxide had a significant effect on the kinetics. Consequently, the adsorption terms can be neglected (K_H=K_C=0), which leads to the rate equation

$$r = \frac{k_{II} K_A c_A {c_0}^2}{(1 + K_A c_A + \frac{k_{II} K_A c_A}{k_{III}})^2} \tag{37}$$

If step III is more rapid than step II, k_{III} dominates over k_{II} and the third term in the denominator can be approximately set to 0. The catalyst is assumed to be stable so that the total number of active sites c_0 is constant. All the constants in the numerator can be summarised to a new constant k'. This leads to the very simplified reaction rate equation for the adsorption-dissociation reaction mechanism,

$$r = \frac{k' c_A}{(1 + K_A c_A)^2} \tag{38}$$

4.4.2. Parameter estimation and quality of the model fit

The rate and adsorption parameters included in the rate Eqs. (28) and (38) were determined by non-linear regression analysis. The ordinary differential equations (ODE) describing the plug flow model (22)-(23) were solved with a stiff ODE solver ODESSA implemented in the software MODEST [19]. The numerical solution of Eq. (22) was repeated several times with different values of the parameters until the minimum of the objective function (Q), i.e. the residual sum of squares was found,

$$Q = \sum_{i=1}^{n} (c_i - c_{i,\exp})^2 \tag{39}$$

A combined simplex-Levenberg-Marquardt method was applied in the search of the minimum of the objective function.

The quality of the fit was investigated by calculating the degree of explanation R^2, which is defined as

$$R^2 = 1 - \frac{\sum_{i=1}^{n} (c_i - c_{i,\exp})^2}{\sum_{i=1}^{n} (c_i - \overline{c_{i,\exp}})^2} \tag{40}$$

Eq. (40) implies that the residual sum of squares Q (Eq. 39) is compared with the simplest possible model, i.e. average value of the concentrations. For a good model fit, typically R^2 values exceeding 0.9 are required. Finally, the identification of the parameters was investigated with Markov Chain Monte Carlo method (MCMC) [20]. The method gives the statistical probabilities of the parameters.

4.5. Modelling results and discussion

The rate parameters in the models were assumed to obey the law of Arrhenius, whereas the adsorption parameter of formic acid was approximated to be independent of temperature. Additionally, to the two rate Eqs. (28) and (38), a very simple first order rate equation was tried for the sake of comparison. Table 1 shows the modelling results for the three different rate equations.

Table 2 displays the rate constant at the mean temperature k', the activation energy E_A and the equilibrium constant K_A. The degree of explanation R^2 helped to determine the quality of the data fit. As expected, the first order model showed the lowest degree of explanation, because it is not based on a reaction mechanism but neglects the impact of formic acid adsorption. The two adsorption models had higher degree of explanation and were quite similar in reproducing the experimental data.

The correlation matrix of the parameters in the adsorption-dissociation model are presented in Table 3. The correlation between the parameters is very moderate, which confirms the statistical reliability of the model. Particularly the correlation between the pre-exponential factor and the activation energy is low, which indicates a good prediction of the temperature dependence of the rate parameter.

The final statistical check of the adsorption-dissociation model was done by performing the MCMC analysis of the parameters. Fig. 12 shows relative profound probabilistic maxima of the model parameters, which supports the results of the non-linear regression analysis.

The following graphical results are presented for the adsorption-dissociation mechanism. The model produces complete concentration profiles inside the reactor. The results for the profiles inside the fixed bed are displayed for the variation of the main process parameters in Figs. 13–15. The fit of the adsorption-dissociation model to the outlet molar flows of the components is compared in the figures below.

The best fit is achieved for the different feed concentrations in Fig. 15, where the deviation between experimental data and the model is very small. The temperature dependence is reflected in Fig. 13. The range of the experimental data points at the outlet is closer than the range of the predicted model. Hence, the influence of the reaction temperature on the experiments is smaller in comparison with the model. The largest deviation between model and experiments is found in Fig. 14, which shows the effect of different flow rates on the molar flows.

The parity plot for the adsorption-dissociation model is shown in Fig. 16, which confirms that no systematic deviations appear between the measured and calculated concentrations. The results of this work supports the adsorption-dissociation mechanism.

5. Conclusions and future perspectives

In this work, the catalytic decomposition of FA was investigated in a laboratory-scale fixed bed reactor. The thermal decomposition of FA was studied in the absence of a catalyst, which resulted in the selection of the temperature 150–225 °C for the kinetic experiments with the Pd/C

catalyst. Within this temperature range, the thermal decomposition is negligible. The influence of the main process parameters was investigated in the systematic kinetic experiments. The experimental data were used for the mathematical modelling of the experimentally recorded decomposition kinetics, for which three different rate equations were tested with non-linear regression analysis. The model based on the adsorption-dissociation mechanism gave a relatively good fit to the experimental data.

The kinetic data set could be improved with the experiences of this work. For instance, experiments at higher reaction temperatures would combine both thermal and catalytic decomposition of FA. The use of a more rapid chromatography might lead to new knowledge, whether the ratio between dehydration and dehydrogenation is time-dependent in a transient operation mode. Additionally, the process could studied by the temperature programmed surface reaction (TPSR) technique to get a deeper insight in the surface reaction mechanism.

CRediT authorship contribution statement

Tapio Salmi: Conceptualization, Methodology, Formal analysis, Writing – original draft, Writing - review & editing, Resources, Project administration, Funding acquisition, Supervision. **Tom Winkler:** Conceptualization, Methodology, Formal analysis, Writing – original draft, Writing – review & editing. **Fabien Baccot:** Methodology, Formal analysis, Writing – review & editing. **Kari Eränen:** Conceptualization, Methodology, Writing – original draft, Resources, Project administration, Supervision. **Johan Wärnå:** Methodology, Formal analysis, Writing – original draft, Writing – review & editing, **Gerd Hilpmann:** Conceptualization, Methodology, Formal analysis, Writing – original draft, Supervision. **Rüdiger Lange:** Conceptualization, Methodology, Formal analysis, Writing – original draft, Supervision. **Markus Peurla:** Methodology, Formal analysis. **Irina Simakova:** Methodology, Formal analysis. **Henrik Grénman:** Conceptualization, Methodology, Formal analysis, Writing – original draft, Project administration. **Tdmitry Murzin:** Conceptualization, Methodology, Formal analysis, Writing – original draft, Writing – review & editing, Supervision.

Declaration of Competing Interest

The authors declare that they have no known competing financial interests or personal relationships that could have appeared to influence the work reported in this paper.

Acknowledgements

This research work is part of the activities financed by Academy of Finland, through the Academy Professor grant 319002 (T. Salmi). Economic support from the Erasmus+ Programme is gratefully acknowledged (T. Winkler, F. Baccot).

Appendix A. Supporting information

Supplementary data associated with this article can be found in the online version at doi:10.1016/j.cattod.2021.10.022.

References

[1] J. Hietala, A. Vuori, P. Johnsson, I. Pollari, W. Reutemann, H. Kieczka, Formic acid. Ullmann's Encyclopedia of Industrial Chemistry, Wiley-VCH Verlag,, Weinheim, 2016, pp. 1–22.
[2] P.G. Jessop, F. Joó, C.-C. Tai, Recent advances in the homogeneous hydrogenation of carbon dioxide, Coord. Chem. Rev. 248 (2004) 2425–2442.
3 OxFA process. Accessed: Jan. 20, 2021. [Online]. Available: ⟨https://www.oxfa.eu/technologie/⟩.
[4] W. Supronowicz, I.A. Ignatyev, G. Lolli, A. Wolf, L. Zhao, L. Mleczko, Formic acid: a future bridge between the power and chemical industries, Green. Chem. 7 (2015) 2904–2911.
[5] A. Züttel, A. Borgschulte, L. Schlapbach, Hydrogen as a future energy carrier, Wiley-VCH,, Weinheim, 2008.
[6] M. Caiti, D. Padovan, C. Hammond, Continuous production of hydrogen from formic acid decomposition over heterogeneous nanoparticle catalysts: from batch to continuous flow, ACS Catal. 9 (10) (2019) 9188–9198.
[7] Eppinger, K.-W. Huang, Formic acid as a hydrogen energy carrier, ACS Energy Lett. 2 (2017) 188–195.
[8] R. Nitzsche, Techno-economic assessment of a wood-based biorefinery concept for the production of polymer-grade ethylene, organosolv lignin and fuel, Bioresour. Technol. 200 (2016) 12–939.
[9] W.M. Goldmann, J. Ahola, M. Mikola, J. Tanskanen, Formic acid aided hot water extraction of hemicellulose from European silver birch (*Betula pendula*) sawdust, Bioresour. Technol. 232 (2017) 19–182.
[10] M. Alvear, A. Aho, I.L. Simakova, H. Grénman, T. Salmi, D. Yu, Murzin, aqueous phase reforming of xylitol and xylose in the presence of formic acid, Catal. Sci. Technol. 10 (2020) 5245–5255.
[11] Q. Luo, G. Feng, M. Beller, H. Jiao, Formic acid dehydrogenation on Ni(111) and comparison with Pd(111) and Pt(111), J. Phys. Chem. C. 116 (2012) 4149–4156.
[12] M.D. Detwiler, C.A. Milligan, D.Y. Zemlyanov, W.N. Delgass, F.H. Ribeiro, Kinetics of gas phase formic acid decomposition on platinum single crystal and polycrystallinen surfaces, Surf. Sci. 648 (2016) 220–226.
[13] P. Mars, J.F. Scholten, P. Zwietering, The Catalytic decomposition of formic acid, 35-113, Adv. Catal. 14 (1963) 35–113.
[14] N. He, Z.H. Li, Palladium-atom catalyzed formic acid decomposition and the switch of reaction mechanism with temperature (Art. no), Phys. Chem. Chem. Phys. 18 (15) (2016) 15–17 (Art. no).
[15] S. Bhandari, S. Rangarajan, C.T. Maravelias, J.A. Dumesic, M. Mavrikakis, Reaction mechanism of vapor-phase formic acid decomposition over platinum catalysts: DFT, reaction kinetics experiments and microkinetic modeling, ACS Catal. 10 (7) (2020) 4112–4126.
16 J.M. Prausnitz and J. Gmehling, Thermodynamik der Phasengleichgewichte, *Verfahrenstechnik* 5, p. XIII–XVI, 1979.
[17] J. Chao, B.J. Zwolinski, Ideal gas thermodynamic properties of methanoic and ethanoic acids, J. Phys. Chem. Ref. Data 7 (1978) 363–377.
[18] T. Salmi, J.-P. Mikkola, P. Wärnå. Chemical reaction engineering and reactor technology, 2nd edition.,, CRC Press Taylor & Francis Group,, Boca Raton, 2019.
[19] H. Haario, MODEST- user's guide, profmath Oy, Helsinki (2011).
[20] H. Haario, M. Laine, A. Mira, E. Saksman, DRAM: efficient adaptive MCMC, Stat. Comput. 16 (2006) 16339–16354.